Electronic Supplementary Information

Adsorption of Two Gas Molecules at a Single Metal Site in a Metal-Organic Framework

Tomče Runčevski, Matthew T. Kapelewski, Rodolfo M. Torres-Gavosto, Jacob D. Tarver, Craig M. Brown and Jeffrey R. Long*

Gas Adsorption

Isotherms were measured on an ASAP 2420 instrument in a sample tube equipped with a Transeal. Tubes were preweighed and samples were transferred into them using a funnel under an atmosphere of N_2. Typically, about 100 mg of sample (post-activation) was in the tube for measurements. Mn_2(dsbdc) samples were activated under dynamic vacuum at pressure of 3 μbar while heating at 150 °C for at least 24 h. UHP-grade (99.999% purity) N_2, H_2, and He were used for adsorption measurements. Warm and cold free spaces were measured using He; N_2 and H_2 isotherms were measured at 77 and 87 K in liquid nitrogen and liquid argon baths, respectively. Oil-free vacuum pumps and pressure regulators were used for all measurements.

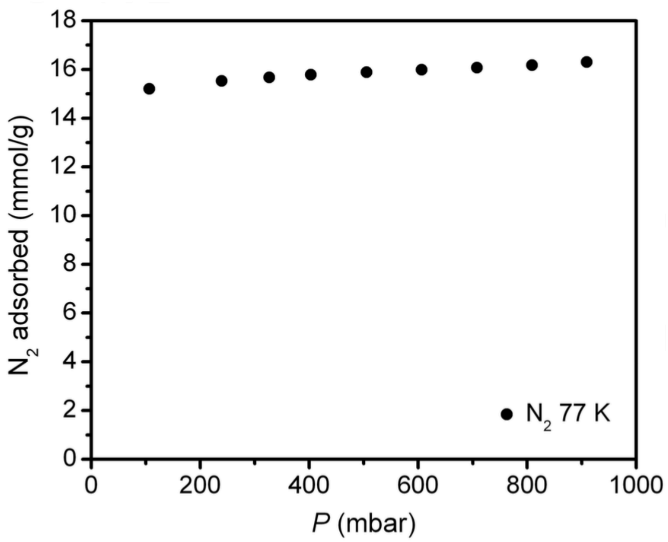

Figure S1. Nitrogen adsorption in the activated Mn_2(dsbdc) sample that was used to calculate a Langmuir surface area of 1605 m^2/g, determined using Micromeritics software.

Langmuir fits

The dual-site Langmuir expression (Equation 1) was used to independently fit the H_2 adsorption data at 77 and 87 K, in which n is the amount adsorbed (mmol/g), q_{sat} is the saturation loading for site A or B (mmol/g), b is the Langmuir parameter associated with either site A or B (bar^{-1}), and p is the pressure (bar).

$$n = \frac{q_{sat,A} b_A p}{1 + b_A p} + \frac{q_{sat,B} b_B p}{1 + b_B p} \qquad (1)$$

The equation was fit using the software program OriginPro 8. The quality of the fits was determined by comparing the adjusted R^2 and residual sum of squares and by visual inspection. Data points at constant loading on each fit were interpolated using Wolfram Mathematica 10, resulting in pressures for each fit at equal loadings. The isosteric heat of adsorption Q_{st} was then calculated using the Clausius-Clapeyron relation (Equation 2). Q_{st} is the isosteric heat of adsorption (kJ/mol), R is the gas constant (kJ·mol^{-1}·K^{-1}), T is the temperature (K), and P is the pressure at either T_1 or T_2 (bar).

$$Q_{st} = -\frac{R[\ln(P_{T_2})-\ln(P_{T_1})]}{T_2^{-1}-T_1^{-1}} \tag{2}$$

Table S1. Dual-site Langmuir equation fit parameters for Mn_2(dsbdc) isotherms at 77 and 87 K.

	77 K	87K
$q_{sat,A}$	8.59	10.03
b_A	0.74	0.83
$q_{sat,B}$	4.67	0.23
b_B	4.33	6.52

Elemental Analysis Table S2. Elemental analysis confirming the 87K 10.03 0.83 0.23 6.52 purity of the activated Mn_2(dsbdc).

	Calculated %	Mn_2(dsbdc) %
C	28.59	28.84
H	0.60	0.48
S	19.08	18.73

Infrared Spectra

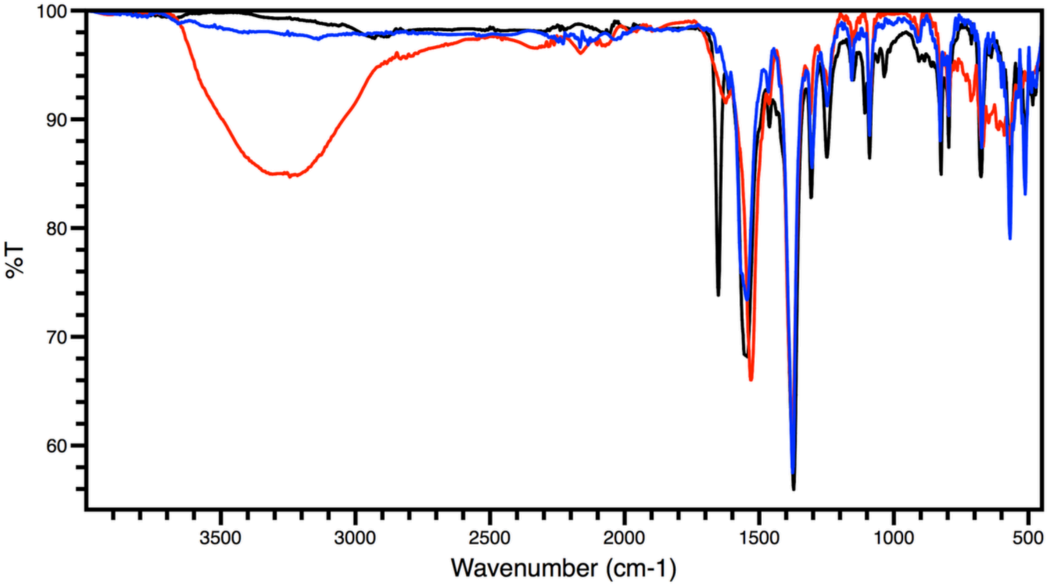

Figure S2. Infrared spectra showing the as-synthesized (black), MeOH-exchanged (red), and activated (blue) Mn_2(dsbdc) samples.

X-ray powder diffraction

High-resolution X-ray powder diffraction patterns of the activated and CO_2 dosed samples of Mn_2(dsbdc) were collected at the 17-BM beamline at the Advanced Photon Source (Argonne National Laboratory) with an average wavelength of 0.72768 Å. X-ray scattered intensity was recorded by a Perkin Elmer a-Si Flat Panel detector at room temperature. The samples were manually powdered in a mortar and pestle under argon atmosphere and sealed in borosilicate glass capillaries of 1 mm (Hilgenberg glass No. 50). The powder data analysis (pattern indexing, profile fitting, crystal structure solution and refinement) was performed with the program TOPAS 4.1.[1]

The indexing of the patterns was done with the singular value decomposition method, [2] resulting in a trigonal unit cell. The space group for both structures was assumed to be *R*-3*c*, which was later confirmed by the structure solution and refinement. Precise lattice parameters were determined by a Pawley fit. [3]

The crystal structure of Mn_2(dsbdc) was solved by the global optimization method of simulated annealing (SA) in real space. [4] For the SA runs a rigid body of half of the dsbdc^{4-} inker was used, together with two Mn^{2+} cations placed at the corresponding special positions implied by the cell symmetry. During the SA runs the *y* fractional coordinate of one Mn^{2+} cation was varied, together with three rotations, three translations for the rigid body. An overall temperature factor for each atom type was included in the SA process. Once a global minimum was found, the crystal structures were subjected to Rietveld refinement, [5] in which bond lengths and angles were refined within the rigid bodies, together with free refinement of all profile and lattice parameters. Hydrogen atoms were added at calculated positions by the program Mercury. [6] Crystallographic details and figures of merit are provided in the deposited CIF.

The crystal structure of the CO_2 dosed Mn_2(dsbdc) sample was solved following the sample procedure only adding two CO_2 molecules described as rigid bodies and keeping the framework structure fixed. The final plot is presented in ESI Figure 3. Crystallographic details and figures of merit are provided in the deposited CIF.

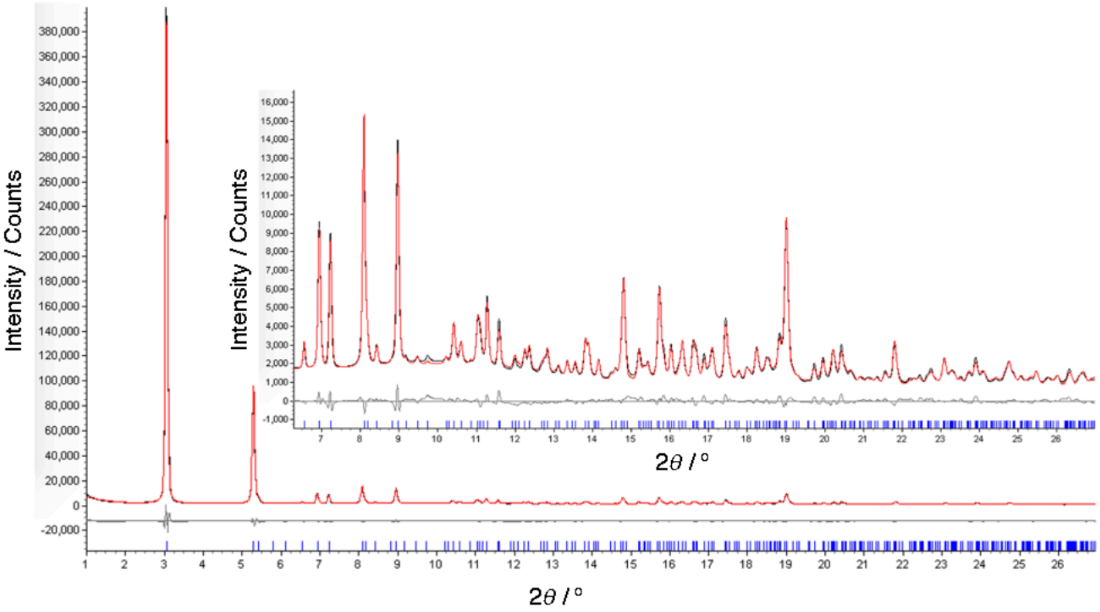

Figure S3. Scattered X-ray intensities as a function of diffraction angle of Mn_2(dsbdc) dosed with 0.13 CO_2 molecules per Mn^{2+} cation, collected at 293 K. The observed pattern (blue line) is measured in Debye-Scherrer geometry. The best Rietveld fit and the difference curve between the observed and the calculated profiles are shown with red and grey lines, respectively. The Bragg reflections positions are presented with vertical blue lines.

Neutron Powder Diffraction

Neutron diffraction measurements were performed on 0.36 g of Mn_2(dsbdc) powder at the National Institute of Standards and Technology Center for Neutron Research (NCNR) using the high-resolution neutron powder diffractometer, BT1. Data was collected using a Ge(311) monochromator with an in-pile 60' collimator, corresponding to a neutron wavelength of 2.0772 Å. To prepare for measurement, the activated sample was transferred to a helium-purged glovebox and loaded into a vanadium sample can. The can was then sealed with an indium o- ring onto a copper heating block containing a valved outlet for gas loading. This assembly was subsequently mounted onto a bottom-loading closed cycle refrigerator and connected to a gas manifold of known volume. Residual helium was evacuated using a turbo-molecular pump prior to measurement.

Diffraction measurements were initially made on the evacuated sample at 10 K. The sample was then heated above 77 K or 120 K and equilibrated at a known dose D_2 or CD_4, respectively. Full adsorption was verified barometrically before cooling to 10 K to avoid condensation prior to diffraction measurement.

Neutron diffraction data was analyzed by the Rietveld method using EXPGUI/GSAS [7]. The starting model for the activated Mn_2(dsbdc) was taken from a structure obtained from synchrotron X-ray diffraction data collected on the bare material at 293 K. For the determination of D_2 and CD_4 adsorption sites, Fourier difference methods were employed to locate adsorbed molecules. An Initial dose of 0.7 D_2 per Mn^{2+} was chosen to minimize potential D2 intermolecular interactions and thereby emphasize the strongest adsorption sites during structural analysis. The structure of the MOF was refined under the constraint of planarity for benzyl rings, and reasonable bond-length/angles for the organic moiety. D_2 was modeled as a D-atom, being allowed to have double occupancy and a large thermal factor to represent the quantum mechanically rotationally disordered molecule as determined previously [8]. After locating the largest scattering nuclear scattering density missing in the Fourier difference, the molecular coordinates of CD4 were initially refined using a rigid body. The orientation of the rigid body only weakly affects he quality of the refinement and the best fit was used in the subsequent step where the CD4 molecular geometry was allowed to relax subject to reasonable bond angle and distance restraints. The MOF framework was fixed at the structure determined for the 0.4 D2:Mn^{2+}. Crystallographic details and figures of merit are deposited as CIFs.

Note: Certain commercial equipment, instruments, or materials are identified in this document. Such identification does not imply recommendation or endorsement by the National Institute of Standards and Technology nor does it imply that the products identified are necessarily the best available for the purpose.

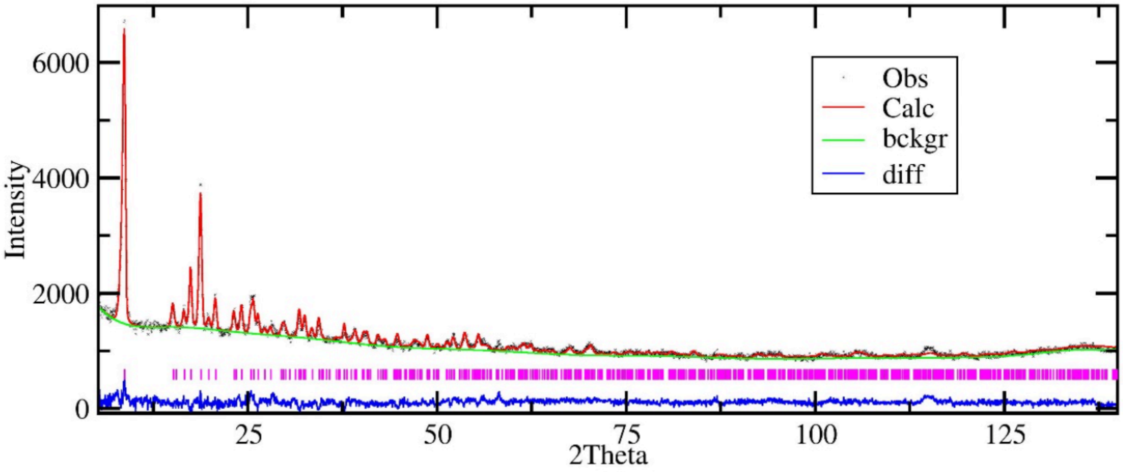

Figure S4. Rietveld refinement of the experimental neutron diffraction pattern (10 K) of evacuated Mn_2(dsbdc) as described in the text. The calculated pattern (red trace) is in good agreement with the experimental data (circles) as evidenced by the difference pattern (blue trace) between calculated and experimental data. Final Rietveld fit parameter was $\chi^2 = 1.398$.

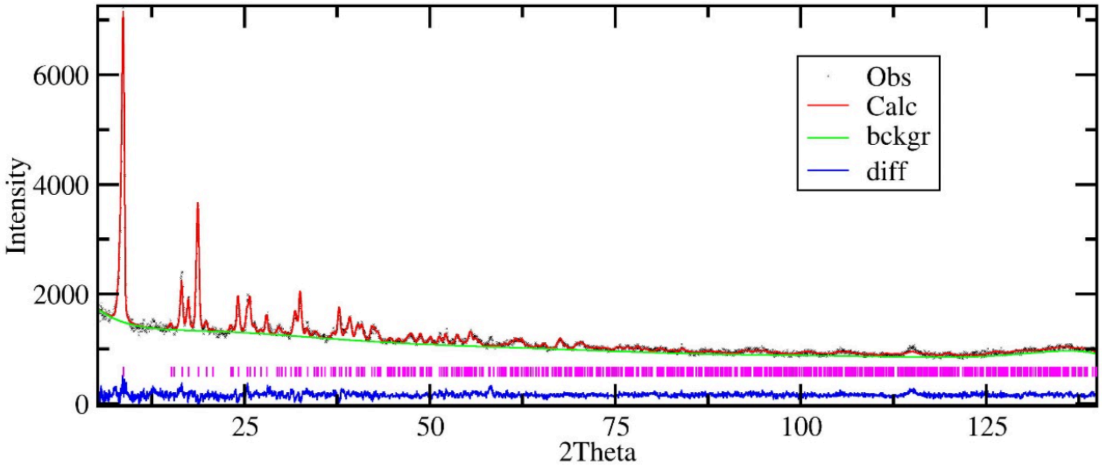

Figure S5. Rietveld refinement of the experimental neutron diffraction pattern (10 K) of evacuated Mn_2(dsbdc) at a loading of 0.75 D_2 per Mn^{2+} as described in the text. The calculated pattern (red trace) is in good agreement with the experimental data (circles) as evidenced by the difference pattern (blue trace) between calculated and experimental data. Final Rietveld fit parameter was $\chi^2 = 1.125$.

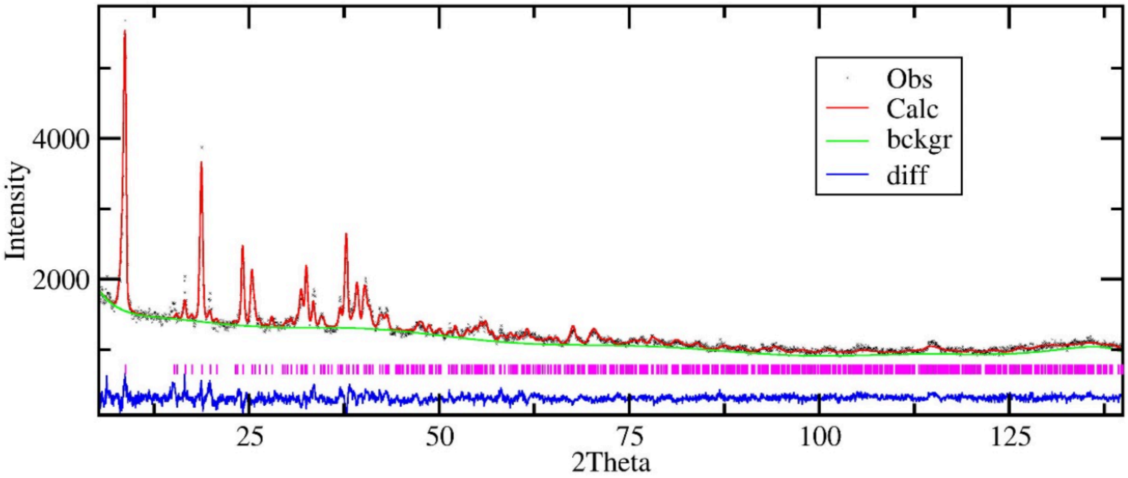

Figure S6. Rietveld refinement of the experimental neutron diffraction pattern (10 K) of evacuated Mn_2(dsbdc) at a loading of 1.4 D_2 per Mn^{2+} as described in the text. The calculated pattern (red trace) is in good agreement with the experimental data (circles) as evidenced by the difference pattern (blue trace) between calculated and experimental data. Final Rietveld fit parameter was χ^2 = 1.359.

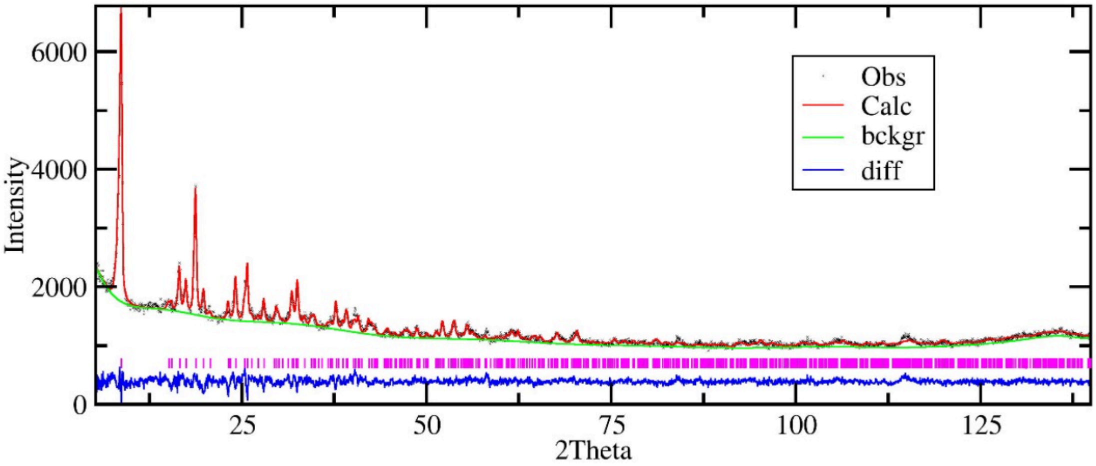

Figure S7. Rietveld refinement of the experimental neutron diffraction pattern (10 K) of evacuated Mn_2(dsbdc) at a loading of 0.4CD_4 per Mn^{2+} as described in the text. The calculated pattern (red trace) is in good agreement with the experimental data (circles) as evidenced by the difference pattern (blue trace) between calculated and experimental data. Final Rietveld fit parameter was χ^2 = 1.465.

Inelastic neutron scattering

Inelastic neutron scattering (INS) spectra were collected using the Filter Analyzer Neutron Spectrometer (FANS) at the NCNR [9] on the same sample used for the NPD experiments. Spectra were collected at 7 K using a pyrolytic graphite (002) monochromatorwith 20’-20’ collimation.

Data were first collected for an activated Mn_2(dsbdc), followed by data collection at loadings of 0.1, 0.2, 0.3, 0.4, 0.5, 0.6, 0.7, 1.0, 1.5, 2.0, and 2.3 H_2 molecules per Mn^{2+} ion.

For gas dosing the sample was always heated to a temperature above which desorption was occurring form the last dosing, or above 77 K for the initial loadings. The sample was subsequently heated to 100 K under dynamic vacuum to evacuate the adsorbed H_2, and was subsequently equilibrated with a dose of 1.0 D_2. Due to the relatively weak binding energy we cooled the sample to 30 K and added an additional 1.0 H_2 per Mn ion. This would ensure that the lower zero-point energy of D_2 would be constrained to occupy the primary adsorption site with a Boltzmann distribution over the weaker sites, and the H_2 mainly adsorbs on the weaker sites. This is a well-known quantum phenomenon that we have taken advantage of several times. [10]

The spectrum of the bare framework was subtracted from the gas-dosed samples and Gaussian peaks were fit to the rotational transitions using the DAVE [11] suite of analysis software. For bulk H_2, the rotational line corresponding to the transitions between rotational quantum numbers $J = 0$ to $J = 1$ is at 14.7 meV. Upon adsorption to a surface the $J = 1$ manifold is split in to its subcomponents that represent details of the site symmetry, strength of adsorption, and overall rotational barrier. [12] These rotational transitions can combine to produce overtones, couple with the vibrational phonon of the H_2 molecule, or phonon modes of the framework leading to high energy transitions that can be complicated to unravel without high level calculations. [13] For the loading of up to 0.7 H_2 : Mn, equivalent to 1.4 H_2 loaded on the available Mn^{2+} ion, the spectra scale indicating the similar adsorption environment through this loading range. There are three rotational transitions located at 9.26(2) meV, 10.96(1) meV, and 12.45(1) meV (for 0.4 H_2:Mn) and then a clear gap where the bulk H_2 rotational line would be before the higher energy modes are apparent. Ideally these peaks should be of identical intensity if the are transitions to the J=1 sublevel, but the details of the spectrometer operation means that there is a momentum transfer (Q) dependence for each energy transfer measured, which would modulate the measured intensity with the expected Q-dependence of the transitions.

With further loading, these low energy features persist and the two lowest energy peaks likely combine whilst there is a simultaneous increase in intensity around 14.7 meV indicative of much weaker adsorption occurring at higher loadings. The shifting of the rotational lines associated the H_2 adsorbed on the Mn indicates that the subsequent weaker adsorption is indeed affecting the local potential of the H_2 associated with the Mn.

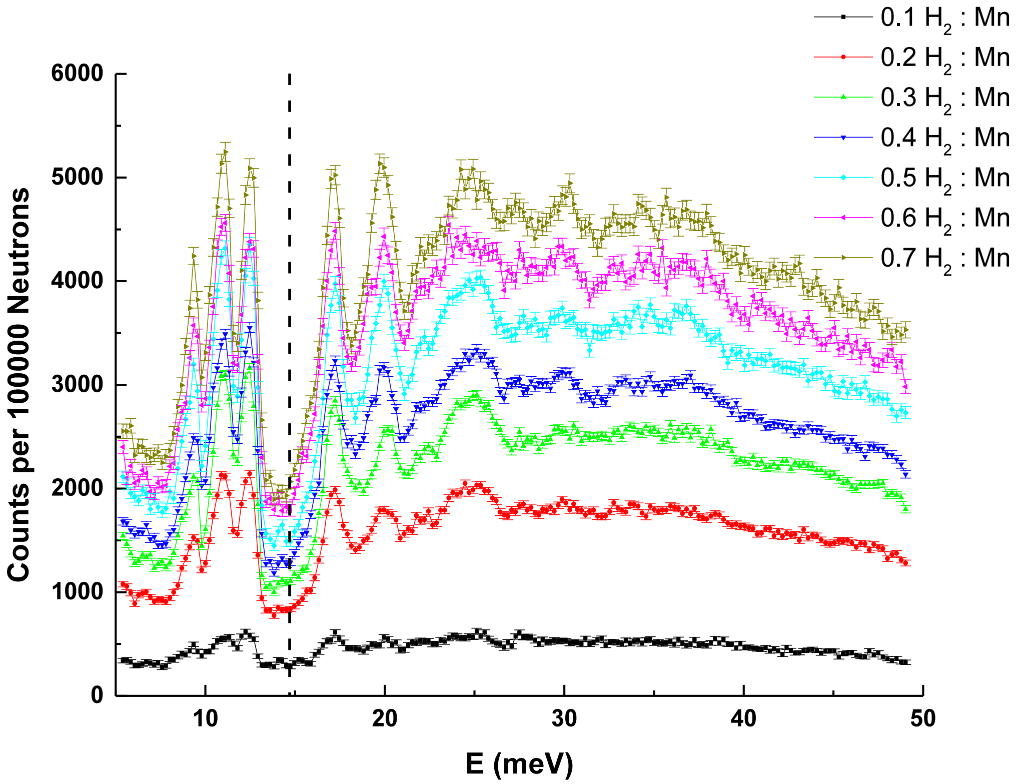

Figure S8. INS data for Mn_2(dsbdc) dosed at loadings of 0.1 (black), 0.2 (red), 0.3 (green), 0.4 (blue), 0.5 (cyan), 0.6 (magenta) and 0.7 (mustard) H_2 molecules per Mn ion. Data are shown after subtraction of bare framework with error bars indicating one standard deviation based on counting statistics. The vertical dashed line indicates the fee-rotor value for H_2.

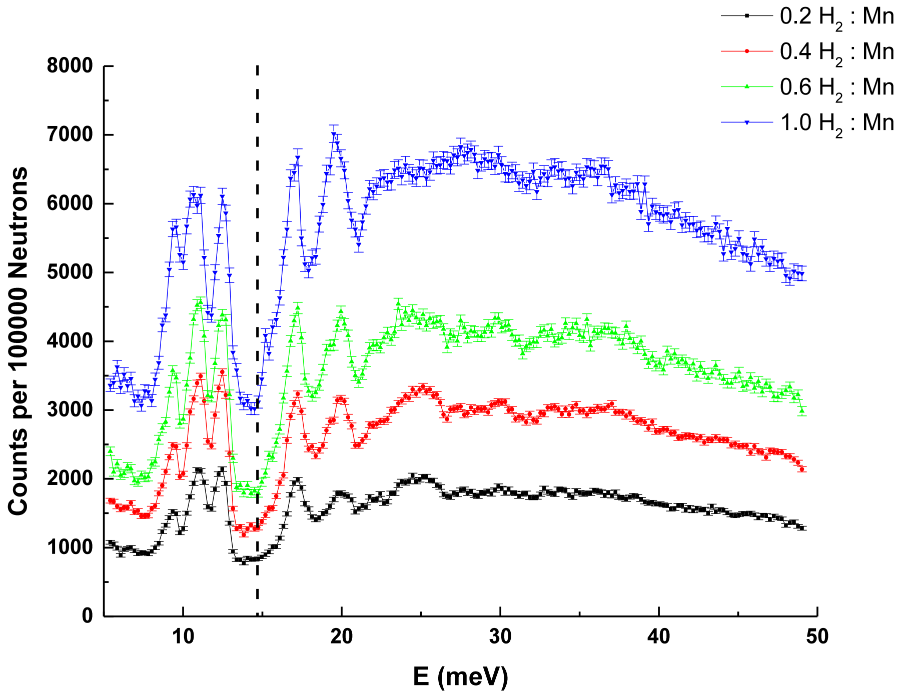

Figure S9. INS data for Mn_2(dsbdc) dosed at loadings of 0.2 (black), 0.4 (red), 0.6 (green) and 1.0 (blue) H_2 molecules per Mn ion. Data are shown after subtraction of bare framework. The vertical dashed line indicates the fee-rotor value for H_2.

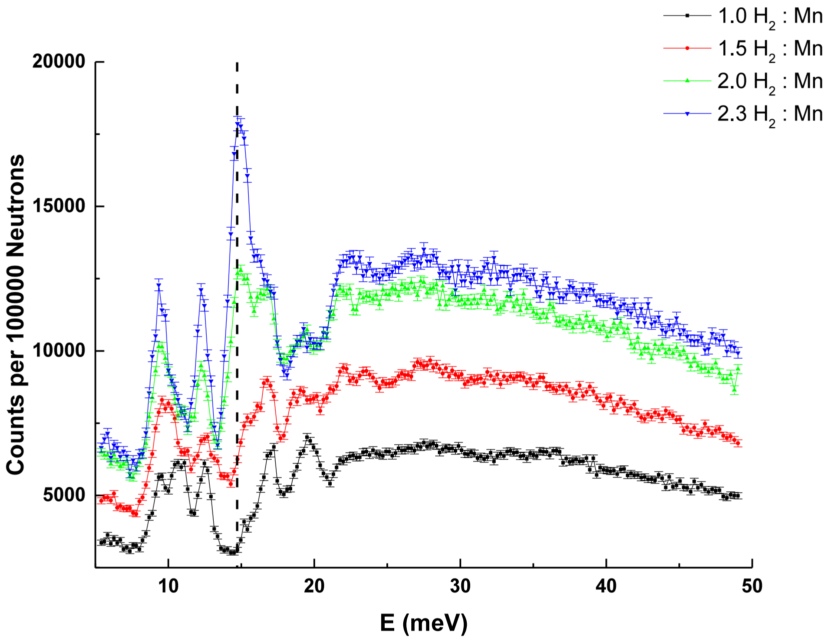

Figure S10. INS data for Mn_2(dsbdc) dosed at loadings of 1.0 (black), 1.5 (red), 2.0 (green) and 2.3 (blue) H_2 molecules per Mn ion. Data are shown after subtraction of bare framework. . The vertical dashed line indicates the fee-rotor value for H_2.

Table S3. INS fitting parameters Mn_2(dsbdc) with the Gaussian center, area and full-width at half-maximum (FWHM).

Loading (H_2 : Mn)	Center (meV)	Area	FWHM (meV)
0.1	9.2 ± 0.1	300 ± 100	1.6 ± 0.3
	11.07 ± 0.06	430 ± 80	1.3 ± 0.2
	12.38 ± 0.04	290 ± 50	0.83 ± 0.09
	17.18 ± 0.05	330 ± 40	1.4 ± 0.1
	19.7 ± 0.1	160 ± 40	1.5 ± 0.3
0.2	9.24 ± 0.02	900 ± 100	1.24 ± 0.08
	10.97 ± 0.01	1980 ± 80	1.32 ± 0.05
	12.42 ± 0.01	1320 ± 50	0.88 ± 0.02
	17.16 ± 0.02	13450 ± 40	1.38 ± 0.04
	19.67 ± 0.04	900 ± 70	1.9 ± 0.1
0.3	9.19 ± 0.02	1300 ± 100	1.22 ± 0.06
	11.00 ± 0.01	3000 ± 100	1.26 ± 0.03
	12.40 ± 0.01	2030 ± 60	0.85 ± 0.02
	17.18 ± 0.01	1970 ± 50	1.34 ± 0.03
	19.86 ± 0.04	1980 ± 80	2.4 ± 0.1
0.4	9.26 ± 0.02	1600 ± 200	1.27 ± 0.07
	10.96 ± 0.01	3400 ± 100	1.33 ± 0.04
	12.45 ± 0.01	2270 ± 60	0.89 ± 0.02
	17.13 ± 0.01	2330 ± 60	1.50 ± 0.03
	19.64 ± 0.02	1670 ± 80	1.66 ± 0.06
0.5	9.21 ± 0.02	1900 ± 200	1.19 ± 0.07
	10.96 ± 0.01	4000 ± 200	1.25 ± 0.04
	12.46 ± 0.01	2830 ± 90	0.88 ± 0.02
	17.16 ± 0.01	2860 ± 80	1.43 ± 0.04
	19.72 ± 0.02	2300 ± 100	1.58 ± 0.06
0.6	9.30 ± 0.03	2600 ± 400	1.5 ± 0.1
	10.96 ± 0.02	3800 ± 200	1.18 ± 0.05
	12.45 ± 0.01	2900 ± 100	0.95 ± 0.03
	17.04 ± 0.02	2800 ± 100	1.40 ± 0.04
	19.57 ± 0.03	1900 ± 200	1.6 ± 0.1
0.7	9.27 ± 0.02	2600 ± 300	1.26 ± 0.8
	10.93 ± 0.01	4600 ± 200	1.24 ± 0.04
	12.48 ± 0.01	3400 ± 100	0.92 ± 0.03
	17.06 ± 0.01	3300 ± 100	1.36 ± 0.04
	19.67 ± 0.02	2700 ± 200	1.48 ± 0.06
1.0	9.47 ± 0.07	4800 ± 900	1.6 ± 0.2

	10.90 ± 0.04	4800 ± 500	1.26 ± 0.09
	12.49 ± 0.02	3900 ± 200	1.063 ± 0.04
	16.90 ± 0.02	2900 ± 200	1.26 ± 0.06
	19.45 ± 0.03	2500 ± 200	1.43 ± 0.09
1.5	9.79 ± 0.02	10900 ± 800	2.29 ± 0.08
	12.43 ± 0.03	3000 ± 300	1.5 ± 0.1
	16.29 ± 0.04	3200 ± 300	1.8 ± 0.1
2.0	9.69 ± 0.04	16000 ± 1000	2.6 ± 0.1
	12.23 ± 0.02	4100 ± 300	1.07 ± 0.05
	15.43 ± 0.03	16100 ± 800	2.92 ± 0.08
2.3	9.58 ± 0.03	19000 ± 2000	2.40 ± 0.09
	12.24 ± 0.01	7400 ± 500	1.07 ± 0.04
	15.12 ± 0.02	23800 ± 700	2.29 ± 0.04
1.0 +1.0 D_2	9.77 ± 0.02	2500 ± 200	1.41 ± 0.05
	12.28 ± 0.01	1800 ± 100	1.08 ± 0.05
	15.46 ± 0.02	7800 ± 200	2.43 ± 0.05

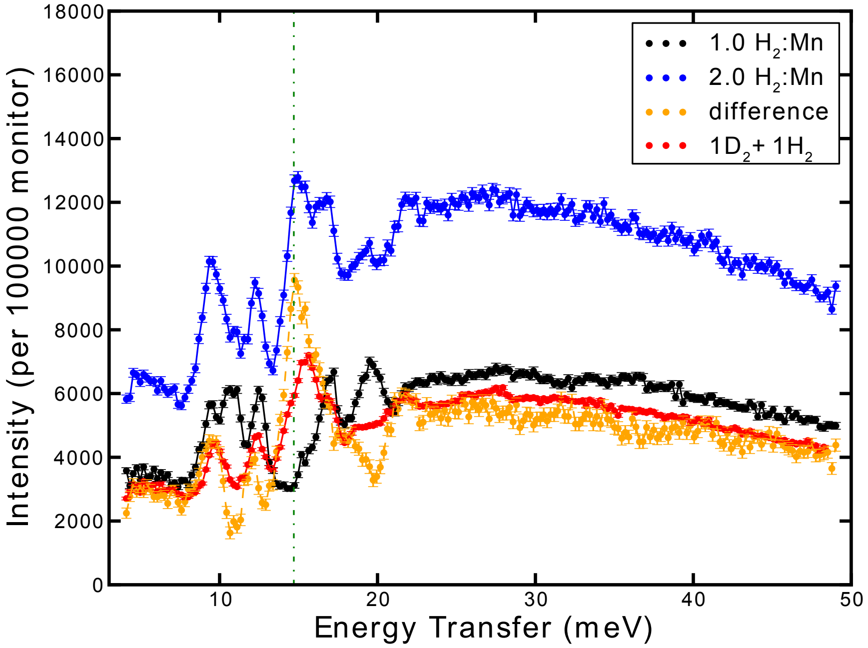

Figure S11. INS data for Mn_2(dsbdc) dosed (and background subtracted) at loadings of 1.0 (black) and 2.0 (blue) H_2 molecules per Mn ion with the difference between them shown in orange. Overlaid in red is the spectrum essentially from the visible H_2 in the D_2:H_2 1:1 mixture that closely resembles the difference spectrum and has the majority of the added hydrogen closely resembling that of solid, bulk-H_2. The vertical dashed line indicates the fee-rotor value for H_2.

References

[1] Bruker AXS, Topas, version 4.1. 2007.

[2] A. A. Coelho, *J. Appl. Cryst.*, 2003, **36**, 86.

[3] G. S. Pawley, *J. Appl. Cryst.*, 1981, **14**, 357.

[4] Y. G. Andreev, G. S. MacGlashan, P. G. Bruce, *Phys. Rev.*, 1997, **B55**, 12011.

[5] H. M. Rietveld, *J. Appl. Crystallogr.*, 1969, **2**, 65.

[6] Mercury CSD 3.3 (Build RC5), 2013.

[7] B. H. Toby, *J. Appl. Crystallogr.* 2001, **34**, 210−213

[8] C.M. Brown, Y. Liu, T. Yildirim, V.K. Peterson, C.J. Kepert*, Nanotechnology*, 2009, **20**, 204025.

[9] T.J. Udovic, C.M. Brown, J.B. Leao, P.C. Brand, R.D. Jiggetts, R. Zeitoun, T.A. Pierce, I. Peral, J.R.D. Copley, Q. Huang, D.A. Neumann, R.J. Fields*, Nuclear Inst. and Methods in Physics Research*, A., 2008, **588**, 406.

[10] W.L. Queen, E.D. Bloch, C.M. Brown, M.R. Hudson, J.A. Mason, L.J. Murray, A.J. Ramirez-Cuesta, V.K. Peterson, J.R. Long*, Dalton Trans.*, 2012, **41**, 4180.

[11] R. T. Azuah, L. R. Kneller, Y. Qui, P. L. W. Tregenna-Piggott, C. M. Brown, J. R. D. Copley, R. M. Dimeo, *J. Res. Natl. Inst. Stand. Technol.*, 2009, **114**, 241.

[12] I.F. Silvera, *Rev. Mod. Phys*., 1980, **52**, 393.

[13] C.M. Brown, Y. Liu, T. Yildirim, V.K. Peterson, C.J. Kepert*, Nanotechnology*, 2009, **20**, 204025.